

# Feedback Linearization Based Nonlinear Control of SynRM Drives Accounting for Self and Cross-Saturation

Angelo Accetta, *Member IEEE*, Maurizio Cirrincione, *Senior Member IEEE*, Marcello Pucci, *Senior Member IEEE*, and Antonino Sferlazza, *Member IEEE*.

**Abstract**—This paper proposes a nonlinear controller based on Feedback Linearization (FL) for Synchronous Reluctance Motors (*SynRM*) drives that takes into consideration the magnetic saturation. The proposed nonlinear FL control based control technique has been developed starting from the theoretical definition of an original dynamic model of the *SynRM* taking into consideration both the self and the cross-saturation effects. Such control technique permits the dynamics of both the speed and direct axis flux loops to be maintained constant independently from the load and the saturation of the iron core in both constant flux and variable direct axis flux operating conditions. Finally, sensitivity of the performance of the proposed FL control versus the variation of the main motor parameters has been further verified. The proposed technique has been tested experimentally on a suitably developed test set-up. The proposed FL control has been further compared with the classic Field Oriented Control (FOC) in both constant flux and variable flux working conditions.

**Index Terms**—Synchronous reluctance motors (*SynRM*), feedback linearization (FL), magnetic saturation.

## I. INTRODUCTION

Synchronous reluctance motors (*SynRM*) have been prototyped around 1923. Their low performance (in terms of output torque and power) combined with their relatively high price have, however, limited their adoption for a long time. Only recently, novel techniques for the advanced design of rotors have permitted increased values of the saliency ratios (9-12), to which the performance of *SynRMs* is strictly related [2]. Nowadays, even if modern *SynRMs* offer output power levels comparable to those of the corresponding Induction Motors (*IM*), very limited number of industries produce them. One of reasons is that due to their constructional characteristics, *SynRMs* can be hardly operated in open loop. High dynamic

performance can be achieved by adopting vector control technique; indeed several Rotor-Oriented Control (*ROC*) or stator Flux-Oriented Control (*FOC*) schemes have been developed [3]–[5]. The theoretical performance of the *SynRMs* is limited, however, by the strong non-linearity of the machine, particularly because of its magnetic characteristics; actually, the saturation phenomena are different on the direct and quadrature axes, and significant cross-saturation phenomena are observable [6].

During these last years several approaches for high-performance control of *SynRM* drives have been developed. In detail, [7] proposed unified direct-flux vector control (*UD-FVC*) scheme adopting a direct stator flux control approach implemented in the stator flux reference frame. The stator flux is directly controlled by the d-axis component of the stator voltage vector, while the torque is controlled by regulating the q-axis component of the stator current vector. The scope of [7] is more to devise a general control scheme to be possibly used for all kinds of motors than to propose a high-performance control technique specifically conceived for *SynRM* drives. In [7] it is explicitly written that a coupling of the quadrature axis current equation with the direct axis exists during flux regulation transients only, which is typical of classic vector controllers. This is a concrete control problem of *SynRM* drives, given that they are typically operated under maximum torque per ampere operation (*MTPA*). The control system theory offers an important set of nonlinear control methodologies for dealing with the nonlinearities of electric motors and try to overcome exactly the above mentioned limits of classic vector controllers.

Among nonlinear control techniques, one of the most promising is the so-called input-output feedback linearization (*FL*) [8], [9]. This issue has been faced up initially with specific regard to induction motor drives [10]–[12]. Nevertheless, very few applications of *FL* to *SynRMs* are still present in the scientific literature [13]–[16]. In particular, [13] proposes an adaptive input-output *FL* technique used for speed and torque-tracking control of a *SynRM* drive, assuming as state variables the direct and quadrature stator flux components and the rotor speed. This controller is capable of estimating on-line the motor static inductances on the two axis. [14] proposed an FL control technique whose main control objective is the minimization of *SynRM* power losses under the constraint of constant torque production. To this aim, [14] includes the iron losses in the *SynRM* model but it neglects the iron saturation

Manuscript received mm dd, yyyy; revised mm dd, yyyy; accepted mm dd, yyyy.

This paper has been previously presented and published, in a preliminary version, in a Conference Proceedings sponsored by the IEEE Industry Application Society: IEEE Energy Conversion Congress and Exposition 2019 (ECCE 2019) [1].

A. Accetta and M. Pucci are with the INstitute for Marine engineering (INM), section of Palermo, National Research Council of Italy (CNR), Via Ugo La Malfa 153, 90146 Palermo, Italy (e-mail: angelo.accetta@cnr.it, marcello.pucci@cnr.it).

M. Cirrincione is with the School of Engineering and Physics, University of the South Pacific, Laucala Campus, 0679 Suva, Fiji (e-mail: cirrincione\_m@usp.ac.fj).

A. Sferlazza is with the Department of Energy, Information engineering and Mathematical models, University of Palermo, Viale delle Scienze, 90128 Palermo, Italy (e-mail: antonino.sferlazza@unipa.it).

phenomenon. In [15] a nonlinear controller is proposed, which directly regulates the torque by selecting the product of  $d$ - and  $q$ -axes currents, concurring to the production of the torque as one of the output variables. In [16] an approach similar to the two previous papers is followed, but only the rotor speed has been estimated. Finally, [17] proposes an input-output feedback linearization technique, permitting the decoupling of the stator flux and electromagnetic torque control loops. In [17] the controller equations are based on the *SynRM* dynamic model expressed in the stator flux reference frame. The dynamic model exploited in [17], however, does not take into account the magnetic saturation.

The input-output Feedback Linearization Control *FLC* technique is, however, a model-based control, and therefore, suffers primarily from two disadvantages: 1) the accuracy of the dynamic model on which the control law is based; and 2) the corresponding correct knowledge of the model parameters. Starting from these remarks, this paper, differently from the previous papers presented in literature, proposes a nonlinear controller based on input-output *FLC* for *SynRMs* drives based on an original accurate dynamic model taking into consideration the self and cross-saturation effects. The proposed *FLC* technique considering the magnetic saturation has been verified experimentally on a suitably developed test setup. It has been experimentally compared with Field Oriented Control (*FOC*), in particular with the Rotor Oriented Control (*ROC*). Experimental tests have been performed in both constant flux and variable flux working conditions. As for the variable flux operation, the *SynRM* drive has been integrated the maximum torque per ampere technique proposed in [18]. Finally, a sensitivity analysis has been made, showing the effects on the performance of the proposed *FLC* of a strong detuning of the main motor parameters (inductances and resistances).

#### A. Comparison with the scientific literature

The proposed *FLC* assumes as state variables the direct and quadrature components of the stator currents and the rotor speed. The space-vector dynamic model on the basis of which the proposed *FLC* has been developed is inspired to [19], whose magnetic model has been proposed in [20], improving it in a far better mathematical description of the cross-saturation phenomenon. As for the control law, the proposed *FLC* follows the approach in [10], [11], where the chosen state variable on the quadrature axis is rotor speed and not the electromagnetic torque. From this point of view, this work differs from [14], [17], where only the stator equations have been linearized by state feedback. In the proposed approach, speed control is performed so that the dynamics of the torque is controlled as internal dynamics of the system, but without the need of a dedicated control loop, as it is the case of *FOC* and *FLC* in [17] in which the controlled variables are torque and flux. The approach in [17] therefore requires the adoption of two controllers on the quadrature axis (torque and speed), whereas the proposed approach requires only one (speed). To follow the proposed approach, the mechanical dynamics of the system, and therefore the inertia of the motor, must be accounted for, to define the suitable set of non-linear transformations of the

Table I  
LIST OF SYMBOLS

SYMBOLS	
$u_{sx}, u_{sy}$	stator voltages in the rotor oriented reference frame;
$i_{sx}, i_{sy}$	stator currents in the rotor oriented reference frame;
$\psi_{sx}, \psi_{sy}$	stator fluxes in the rotor oriented reference frame;
$L_{sxx}, L_{syy}$	self static inductances along $x$ and $y$ axes;
$L_{sxy}, L_{syx}$	cross static inductances;
$L'_{sxx}, L'_{syy}$	self dynamic inductances along $x$ and $y$ axes;
$L'_{sxy}, L'_{syx}$	cross dynamic inductances;
$R_s$	stator resistance;
$\omega_r$	angular speed of the rotor (mechanical angles);
$t_m$	electromagnetic torque generated by the motor;
$t_l$	load torque;
$p$	pole-pairs;
$J$	rotor inertia;
$f_v$	viscous friction coefficient.

states and inputs. As for the *FLC* proposed in [13], since it assumes the stator flux components as state variables besides the speed, it reveals necessarily simpler than the proposed one, regarding the dynamic model. Moreover, it presents the advantage of being adaptive with the variation of the direct and quadrature static inductances. This advantage is, however, paid by the fact that the control system requires online knowledge of the stator flux direct and quadrature components. These quantities cannot be measured online while they are to be estimated by flux models or observers. The control system performance and the accuracy in the estimation of the inductances in [13], thus, suffers also from the accuracy of the stator flux components by the flux model. On the contrary, the proposed *FLC* requires the online knowledge of the stator current components, which are measured quantities and thus it is intrinsically more accurate than [13] and potentially more performing. Finally, all the works in literature dealing with the *FLC* of *SynRMs* do not consider the self and cross-saturation effects to the best of the authors' knowledge, and this is one of the major contributions of this work.

## II. SPACE-VECTOR STATE MODEL OF THE *SynRM* CONSIDERING SELF AND CROSS-SATURATION

A complete magnetic model of the *SynRM* has been proposed in [20], where specific original flux versus current functions have been deduced, permitting both the self and cross-saturation effects to be accounted for. Correspondingly, [19] proposed a new space-vector model of the *SynRM* including self and cross-saturation effects, expressed in state form. The definition of such a model is crucial for developing the nonlinear feedback linearization technique proposed in this paper. The magnetic model proposed in [19] has been significantly improved here in order to better describe the cross-saturation phenomenon.

#### A. Literature Review of Magnetic Models of *SynRMs*

[21] presents a review of some explicit functions for modeling the magnetic saturation of *SynRM*, dividing them into two major approaches: the flux vs current, to be used when the current is assumed as a state variable and the current versus flux ones, to be used when the flux is assumed as the

state variable. As for the current versus flux approach, two kinds of functions are cited: 1) the power function [22], 2) the arctan function (modeling the derivative of the current to the flux and thus to be integrated) [23]. None of them, however, accounts for the cross-saturation phenomenon. As for the flux versus current approach, three kinds of functions are cited: 1) Piecewise Functions proposed in [24] for describing only the self-saturation and improved in [25] by integrating the cross-saturation, 2) the polynomial functions [26] accounting for the cross-saturation, the rational functions [27] accounting for the cross-saturation but not fulfilling the reciprocity conditions. In particular, [21] proposes a magnetic model belonging to the current vs flux approach and based on an improved version of the power function accounting also for the cross-saturation and respecting the reciprocity condition. In [28] the authors address the issue of the experimental magnetic characterization of the flux versus current relationship of *IPMs* and *PM* assisted *SynRMs*. In particular, a simplified but effective model of the cross-saturation phenomenon is proposed.

### B. Proposed magnetic model

The proposed magnetic model is in the framework of a flux versus current approach, so it is suitable for dynamic models of *SynRMs* adopting the stator currents as state variables. As for the magnetic characteristics of the *SynRM*, the following functions are proposed, which consider both the self and cross-saturation effects and describe the relationships between the direct and quadrature components of the stator fluxes and the corresponding components of the stator currents in the synchronous reference frame. The stator flux direct ( $x$ ) and quadrature ( $y$ ) components have been defined as follows:

$$\psi_{sx} = 2\alpha_1 \left( \frac{1}{1 + e^{-\beta_1 i_{sx}}} - \frac{1}{2} \right) + \eta_1 i_{sx} + \Delta\psi_{sx} \quad (1a)$$

$$\psi_{sy} = 2\alpha_2 \left( \frac{1}{1 + e^{-\beta_2 i_{sy}}} - \frac{1}{2} \right) + \eta_2 i_{sy} + \Delta\psi_{sy} \quad (1b)$$

In particular, as for the self-saturation, it has been formulated adopting sigmoid functions, to which linear functions are added because the magnetic characteristic of the motor is not completely flat in deep saturation. As for the cross-saturation, it has been conceived starting from the definition of a proper co-energy variation function due to the cross-saturation. The co-energy variation function has been expressed as the product of two functions, one depending only on  $i_{sx}$  and the other depending only on  $i_{sy}$ . This last condition is very important since it permits the reciprocity conditions to be properly fulfilled. The mathematical formulation has been created based on the analysis of [29, Fig. 2]. This last figure shows that the flux on the  $x$  axis reduces for increasing values of the current  $i_{sy}$ . Moreover, for a given value of  $i_{sx}$ , the amount of reduction of the flux on the  $x$  axis depends on the absolute value of  $i_{sy}$ , being independent from its sign. The higher the absolute value of  $i_{sy}$  is, the higher the flux reduction on the  $x$  axis is. Moreover, the same figure shows that the flux variation on the  $x$  axis is null for zero value of  $i_{sx}$ , very little for high values of  $i_{sx}$ , while it presents a maximum for a certain intermediate range of  $i_{sx}$ . These considerations suggest that

the flux variation on the  $x$  axis should be weighted with a function of  $i_{sx}$  presenting a bell shape. Since it is needed that such a function presents a primitive (for the definition of the co-energy variation function), it has been chosen the derivative of the sigmoid function, which is a combination of exponentials. In particular, the defined co-energy variation functions is the following:

$$\Delta W' = \gamma \frac{1}{\left(1 + e^{\frac{-(i_{sx} - \mu_1 \operatorname{sgn}(i_{sx})) \operatorname{sgn}(i_{sx})}{\sigma_1}}}\right)} \frac{1}{\left(1 + e^{\frac{-(i_{sy} - \mu_2 \operatorname{sgn}(i_{sy})) \operatorname{sgn}(i_{sy})}{\sigma_2}}}\right)}. \quad (2)$$

From (2) the cross-saturation flux variation terms can be computed as:

$$\Delta\psi_{sx} = \frac{d\Delta W'}{di_{sx}} = -l_{xx} l_{xy}, \quad (3a)$$

$$\Delta\psi_{sy} = \frac{d\Delta W'}{di_{sy}} = -l_{yy} l_{yx}, \quad (3b)$$

where  $l_{xx}$ ,  $l_{xy}$ ,  $l_{yy}$  and  $l_{yx}$  are given in the Appendix.

Since the nonlinear inductor should not generate or dissipate electrical energy, the reciprocity condition must be satisfied [21], [30], and the cross-saturation dynamic inductance can be coherently defined as:

$$L'_{sxy} = \frac{d\Delta\psi_{sx}}{di_{sy}} = \frac{d\Delta\psi_{sy}}{di_{sx}} = -\frac{1}{\gamma} l_{xx} l_{yy}. \quad (4)$$

The analysis of Eq. (4) shows that, independently from the numerical values of the parameters, the signs requirements described in [31] are satisfied. Finally, the self-saturation dynamic inductances on the direct and quadrature axis can be defined as:

$$L'_{sxx} = \frac{d\psi_{sx}}{di_{sx}} = \eta_1 + \frac{2\alpha_1 \beta_1}{\left(e^{\frac{\beta_1 i_{sx}}{2}} + e^{-\frac{\beta_1 i_{sx}}{2}}\right)^2} + \frac{1}{\sigma_1} \operatorname{sgn}(i_{sx}) l_{xx} l_{xy} l'_x, \quad (5a)$$

$$L'_{syy} = \frac{d\psi_{sy}}{di_{sy}} = \eta_2 + \frac{2\alpha_2 \beta_2}{\left(e^{\frac{\beta_2 i_{sy}}{2}} + e^{-\frac{\beta_2 i_{sy}}{2}}\right)^2} + \frac{1}{\sigma_2} \operatorname{sgn}(i_{sy}) l_{yy} l_{yx} l'_y, \quad (5b)$$

where  $l'_x$  and  $l'_y$  are given in the Appendix.

As for the static inductances, they are straightforwardly defined as:

$$L_{sxx} = \frac{\psi_{sx}}{i_{sx}} = \eta_1 + 2\alpha_1 \left( \frac{1}{1 + e^{-\beta_1 i_{sx}}} - \frac{1}{2} \right) \frac{1}{i_{sx}} - \frac{l_{xx} l_{xy}}{i_{sx}}, \quad (6a)$$

$$L_{syy} = \frac{\psi_{sy}}{i_{sy}} = \eta_2 + 2\alpha_2 \left( \frac{1}{1 + e^{-\beta_2 i_{sy}}} - \frac{1}{2} \right) \frac{1}{i_{sy}} - \frac{l_{yy} l_{yx}}{i_{sy}}. \quad (6b)$$

The entire magnetic behavior of the machine can be, therefore, described by functions requiring the knowledge of 11 model

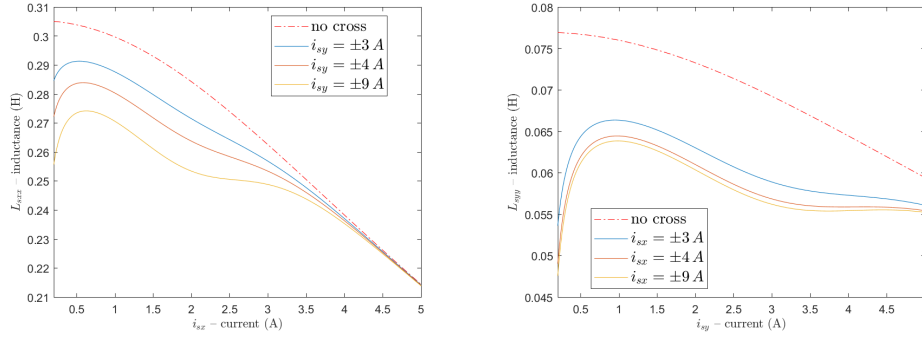


Figure 1. Static self-inductance on the direct axis,  $L_{sxx}$ , and on the quadrature axis,  $L_{syy}$ , for several values of the current.

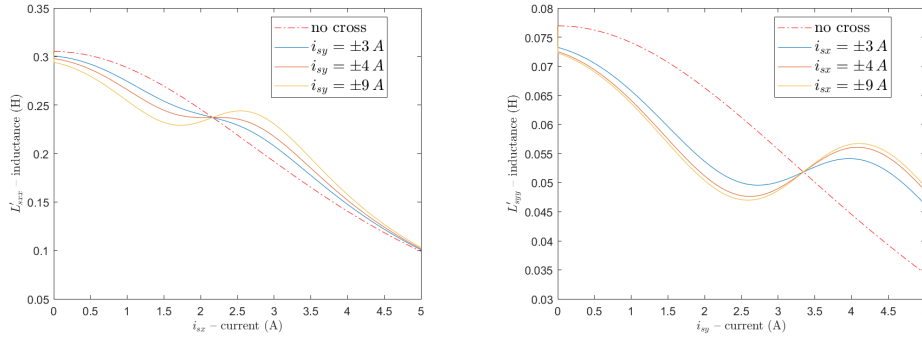


Figure 2. Dynamic self-inductance on the direct axis,  $L'_{sxx}$ , and on the quadrature axis,  $L'_{syy}$ , for several values of the current.

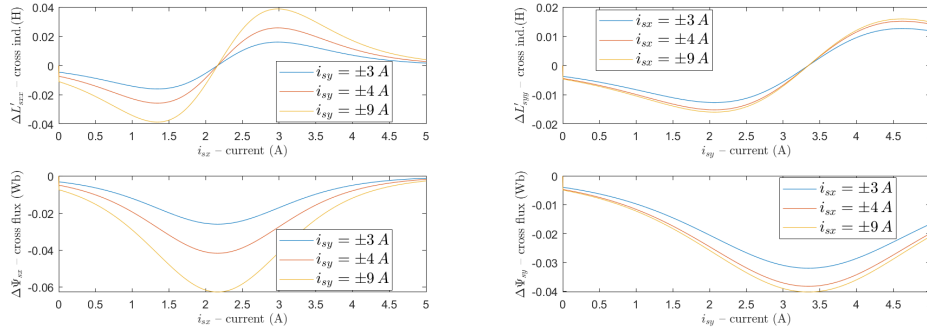


Figure 3. Cross saturation terms of the dynamic self-inductance on the direct and quadrature axis for several values of the current (top plots) and cross saturation flux (bottom plots).

parameters ( $\alpha_1, \beta_1, \eta_1, \gamma, \mu_1, \sigma_1, \alpha_2, \beta_2, \eta_2, \mu_2$  and  $\sigma_2$ ), 6 describe the self-saturation on both axes ( $\alpha_1, \beta_1, \eta_1, \alpha_2, \beta_2, \eta_2$ ) and 5 describe the cross-saturation ( $\gamma, \mu_1, \sigma_1, \mu_2$  and  $\sigma_2$ ). The parameters of the proposed, have been identified adopting the methodology presented in [32].

As for the *SynRM* under test, whose photo is shown in Fig. 9 and rated values and model's parameters are described in Tab.s IV and V, Fig. 1 shows the variation of the static self-inductance on the direct (quadrature) axis versus the direct (quadrature) axis current for several values of the quadrature (direct) current, defined in Eq.s (6). These figures show a set of curves, obtained respectively for zero current on the other axis (no cross-saturation is present) as well as for increasing values of the current on the other axis. It can be observed that  $L_{sxx}$  decreases with  $i_{sx}$ , as expected because of the self-saturation

phenomenon. It can be further observed that  $L_{sxx}$  decreases for increasing values of  $i_{sy}$ . The higher  $i_{sy}$  is the lower  $L_{sxx}$  is; in particular, the inductance curves obtained with nonnull values of  $i_{sy}$  is lower than that obtained with null value of  $i_{sy}$  for any value of  $i_{sx}$ . The same phenomenon is observable on  $L_{syy}$ . As for the dynamic self-inductance defined in Eq.s (5), Fig. 2 shows the variation of the dynamic self-inductance on the direct (quadrature) axis versus the direct (quadrature) axis current for several values of the quadrature (direct) current. The shapes of dynamic inductances are similar to those of the static ones, with some differences highlighted in the following. It can be observed that the direct axis dynamic self-inductance curve obtained for nonnull values of quadrature axis current, below a certain current threshold and for increasing values of the direct axis current, is lower than that obtained for zero

quadrature axis current (no cross-saturation). The reason is the reduction of the direct axis flux caused by the further saturation of the self-axis by the quadrature current. The shape of the dynamic self-inductance above this threshold of direct axis current changes. In fact, the direct axis flux reduction caused by the cross-saturation is not equal in the entire range of the direct axis current. It is null for zero direct axis current, then it increases getting a maximum, and then it starts decreasing to a limited value because the magnetic circuit is already fully saturated by the direct axis current. On the quadrature axis the self-flux reduction due to the direct axis current, above a certain value of quadrature current, is less observable. This phenomenon is coherent with the fact that the quadrature axis magnetic circuit gets less easier the full saturation. The above-described kind of variation is confirmed also in [29, Fig. 2]. As for the proposed magnetic model, such a phenomenon is shown in Fig. 3 (bottom plots), showing the flux reduction on both axis caused by the cross-saturation. Since the dynamic direct axis self-inductance is defined as the derivative of the direct axis flux with respect to the direct axis current, the component of the direct axis dynamic self-inductance due to the cross saturation changes its sign above a certain value of direct axis current (see Fig. 3 top plots). This phenomenon finally motivates why a certain value of direct axis current exists, above which the direct axis dynamic self-inductance obtained with a non-null value of the quadrature axis current becomes higher than that obtained for zero quadrature axis.

The proposed *FLC* control technique assumes an a priori knowledge of the magnetic behavior of the *SynRM*. This is a slight complication of the control law, all the inductance functions have to be implemented on-line, and thus the related parameters must be previously off-line identified. In the authors' opinion, however, this does not limit the application of the proposed method to other machines with different ratings. As a matter of fact, the methodology for off-line identifying the model parameters defined in [20], is based on 3 simple stand still tests, that do not require the machine to be run at any speed or load. The tests just require the *SynRM* to be supplied by a voltage source inverter, that is something implicit in its adoption. The off-line identification procedure can be easily integrated in the control action as a preliminary self-commissioning phase, within which even the controllers tuning can be included. In general, a proper tuning of the current regulators of a *SynRM* drive would require, in any case, a proper magnetic characterization of the machine.

The static and dynamic inductance surfaces function, if straightforward implemented, would require a very high computational demand. In this case, however, all these surfaces have been experimentally implemented as linearly interpolated functions, thus reducing significantly the computational demand.

### C. Dynamic model of the *SynRM*

If  $\Psi_s = [\psi_{sx}, \psi_{sy}]$  is the vector whose elements are the direct and quadrature stator flux components in the rotor reference frame, and  $\mathbf{i}_s = [i_{sx}, i_{sy}]$  is the corresponding stator current components vector, the complete space-vector dynamic

model of the *SynRM* in state form, selecting the stator fluxes as state variables, can be written as:

$$\frac{d\Psi_s}{dt} = \mathbf{u}_s - R_s \mathbf{i}_s - j\omega_r \Psi_s. \quad (7)$$

The stator current can be obtained from the stator fluxes by means of the following relations:

$$i_{sx} = L_{sxx}^{-1} \psi_{sx}, \quad i_{sy} = L_{syy}^{-1} \psi_{sy}, \quad (8)$$

where the expression of  $L_{sxx}$  and  $L_{syy}$  are given in (6).

By replacing (6) into Eqs. (8), and properly differentiating, model (7) can be also conveniently written by considering the stator currents as state variables, instead of the stator fluxes, as follows:

$$\frac{d\mathbf{i}_s}{dt} = \mathbf{L}'_s{}^{-1} (\mathbf{u}_s - R_s \mathbf{i}_s - jp\omega_r \Psi_s). \quad (9)$$

The inverse matrix of the dynamic inductances in (9) is defined as:

$$\mathbf{L}'_s{}^{-1} = \frac{1}{L'_{sxx}L'_{syy} - L'_{sxy}{}^2} \begin{bmatrix} L'_{sxx} & -L'_{sxy} \\ -L'_{sxy} & L'_{syy} \end{bmatrix}, \quad (10)$$

where  $L'_{sxx}$ ,  $L'_{syy}$  and  $L'_{sxy}$  and their expressions are given in (4) and (5).

Finally the mechanical equation of the *SynRM* is given by:

$$J \frac{d\omega_r}{dt} = -f_v \omega_r + t_m - t_l, \quad (11)$$

where  $J$  and  $f_v$  are the moment of inertia and the viscous friction coefficient,  $t_l$  is the load torque, and  $t_m$  is the electromagnetic torque produced by the motor given by:

$$\begin{aligned} t_m &= \frac{3}{2}p (\psi_{sx}i_{sy} - \psi_{sy}i_{sx}) = \frac{3}{2}p (L_{sxx} - L_{syy}) i_{sx}i_{sy} \\ &= \frac{3}{2}p \left( \frac{1}{L_{syy}} - \frac{1}{L_{sxx}} \right) \psi_{sx}\psi_{sy}. \end{aligned} \quad (12)$$

It is noteworthy that only the expression of the static inductances appears in the dynamics of the speed, since the electromagnetic torque is explicitly dependent on the static inductances, and it depends on the dynamic inductances only indirectly through the stator fluxes.

## III. NONLINEAR CONTROLLER DESIGN

Let's suppose that the *SynRM* drive is operated under *ROC* or *FOC* or any *FLC* not involving the speed loop in the controller design. If the controlled variable are the direct axis current (proportional to the direct axis flux by the direct static self-inductance) and the rotor speed, assumed that the drive is operated under *MTPA* (variable direct axis current), the speed and the direct axis control loops are coupled by the torque expression (12). The only way to decouple the speed and direct axis current loops is to adopt a suitably defined *FLC* accounting for the mechanical dynamic equation. In the following the proposed approach is described. To design the controller, equations (7), (9) and (11) are now considered. Moreover, the two outputs of this model are represented by the direct axis flux,  $\psi_{sx}$ , and the mechanical speed  $\omega_r$ . Note that this system is a *MIMO* system, therefore a state feedback will be designed so that the resulting system can be viewed

as two decoupled systems: the first governs the  $\psi_{sx}$  dynamics and the second governs the  $\omega_r$  dynamics. Finally, the target of the proposed controller is the full decoupling between these two systems in any operating condition, independently of the load and the saturation condition.

With regard to the direct axis flux dynamics, if the Lie derivative of  $\psi_{sx}$  is computed, the first equation of (7) is obtained. This means that if the state vector is defined as:

$$x := [i_{sx} \quad i_{sy} \quad \omega_r]^\top, \quad (13)$$

and the input  $u_{sx}$  is designed such that:

$$u_{sx} = R_s i_{sx} - \omega_r \psi_{sy} + \nu_x := f_1(x) + \nu_x, \quad (14)$$

then the dynamics of  $\psi_{sx}$  can be written in terms of the new input  $\nu_x$  as follows:

$$\frac{d\psi_{sx}}{dt} = \nu_x. \quad (15)$$

With regards to the speed dynamics, if the new state variable  $a$ , called *acceleration* and defined as  $a := \frac{d\omega}{dt}$ , is introduced, then it is possible to compute the second order Lie derivative of the speed along the trajectories of the system as follows:

$$\frac{d\omega^2}{dt^2} = -\frac{f_v}{J}a + \frac{3p}{2J} \left( [g_1 \quad g_2] \mathbf{L}'_s^{-1} + \left( \frac{1}{L_{sy}} - \frac{1}{L_{sx}} \right) [\psi_{sy} \quad \psi_{sx}] \right) [u_{sx} - R_s i_{sx} + \omega_r \psi_{sy}], \quad (16)$$

where:

$$g_1 := \left( \frac{\partial L_{sxx}}{\partial i_{sx}} - \frac{\partial L_{syy}}{\partial i_{sx}} \right) = \frac{1}{i_{sx}} \left( \frac{L'_{sxx} - L_{sxx}}{L_{sxx}^2} \right) + \frac{1}{i_{sy}} \left( \frac{L'_{syy}}{L_{syy}^2} \right), \quad (17a)$$

$$g_2 := \left( \frac{\partial L_{sxx}}{\partial i_{sy}} - \frac{\partial L_{syy}}{\partial i_{sy}} \right) = \frac{1}{i_{sy}} \left( \frac{L'_{syy} - L_{syy}}{L_{syy}^2} \right) + \frac{1}{i_{sx}} \left( \frac{L'_{sxy}}{L_{sxx}^2} \right). \quad (17b)$$

As can be seen from Eq. (16), both the input  $u_{sx}$  and  $u_{sy}$  appear in the expression. Then the model in this form cannot be feedback linearizable in the "classical" form since the dynamic of speed cannot be made independent of the control of  $\psi_{sx}$ . However, from equations (14)-(15) it is apparent that the dynamics of  $\psi_{sx}$  does not depend on  $u_{sy}$ . This suggests considering the two systems as a cascade of two subsystems: the first that describes the  $\psi_{sx}$  dynamics and the second that describes the  $\omega_r$  dynamics. In this way, it is possible to design  $\nu_x$  (and consequently  $u_{sx}$  by (14)) in order to assign the dynamics of (15), and then to consider  $\nu_x$  as a time-varying quantity that perturbs the second subsystem (the one of the speed). Obviously,  $\nu_x$  is known and it will be necessary to compute the feedback law to linearize the speed dynamics. In other words the following is defined:

$$u_{sy} = R_s i_{sy} + \omega_r \psi_{sx} + \bar{\nu}_y := f_2(x) + \bar{\nu}_y, \quad (18)$$

and by considering Eq. (14), then Eq. (16) can be written as:

$$\frac{d\omega^2}{dt^2} = -\frac{f_v}{J}a + \frac{3p}{2J} (h_1(x)\nu_x + h_2(x)\bar{\nu}_y), \quad (19)$$

where:

$$h_1(x) := \frac{g_1 L'_{sxx} + g_2 L'_{sxy}}{L'_{sxx} L'_{syy} - L'_{sxy}{}^2} + \left( \frac{1}{L_{sy}} - \frac{1}{L_{sx}} \right) \psi_{sy}, \quad (20a)$$

$$h_2(x) := \frac{g_1 L'_{sxy} + g_2 L'_{syy}}{L'_{sxx} L'_{syy} - L'_{sxy}{}^2} + \left( \frac{1}{L_{sy}} - \frac{1}{L_{sx}} \right) \psi_{sx}. \quad (20b)$$

At this point, it is possible to define the auxiliary input  $\bar{\nu}_y$  as:

$$\begin{aligned} \bar{\nu}_y &:= h_2^{-1}(x) \left( -h_1(x)\nu_x + \frac{2J}{3p} \left( \frac{f_v}{J}a + \nu_y \right) \right) \\ &= h_2^{-1}(x) \left( -h_1(x)\nu_x + \frac{2J}{3p} (f_3(x) + \nu_y) \right), \end{aligned} \quad (21)$$

with:

$$f_3(x) := \frac{f_v}{J^2} \left( \frac{3}{2} p \left( \frac{1}{L_{sy}} - \frac{1}{L_{sx}} \right) \psi_{sx} \psi_{sy} - f_v \omega_r - t_l \right), \quad (22)$$

where  $\nu_y$  is a new auxiliary input. With the above definition, the system describing the speed dynamics, becomes:

$$\frac{d\omega_r}{dt} = a, \quad \frac{da}{dt} = \nu_y, \quad (23)$$

which appears in the standard linear form.

Note that each state function  $f_1(x)$ ,  $f_2(x)$ ,  $f_3(x)$ ,  $h_1(x)$  and  $h_2(x)$ , appearing in the scheme of Fig. 4, can be conveniently written as only function of the currents  $i_{sx}$ ,  $i_{sy}$ , and the speed  $\omega_r$ , which are all measurable quantities. Indeed, by considering the above given relationships, it is possible to write:

$$f_1(x) := R_s i_{sx} - \omega_r L_{syy} i_{sy}, \quad (24a)$$

$$f_2(x) := R_s i_{sy} + \omega_r L_{sxx} i_{sx}, \quad (24b)$$

$$f_3(x) := \frac{f_v}{J^2} \left( \frac{3}{2} p (L_{sxx} - L_{syy}) i_{sx} i_{sy} - f_v \omega_r - t_l \right), \quad (24c)$$

$$h_1(x) := \frac{g_1 L'_{sxx} + g_2 L'_{sxy}}{L'_{sxx} L'_{syy} - L'_{sxy}{}^2} + \left( 1 - \frac{L_{syy}}{L_{sxx}} \right) i_{sy}, \quad (24d)$$

$$h_2(x) := \frac{g_1 L'_{sxy} + g_2 L'_{syy}}{L'_{sxx} L'_{syy} - L'_{sxy}{}^2} + \left( \frac{L_{sxx}}{L_{syy}} - 1 \right) i_{sx}. \quad (24e)$$

where  $g_1$  and  $g_2$ , given in (17), as well as the static and dynamic inductances, given in (4), (5) and (6), are already expressed as function of the currents  $i_{sx}$  and  $i_{sy}$ .

*Remark 1:* The proposed control scheme requires the existence of the inverse of  $h_2(x)$ ,  $h_2^{-1}(x)$ . However, it is possible to prove that the inverse exists if  $\psi_{sx} \neq 0$  and this condition is always satisfied, because the *SynRM* works properly only if the direct axis flux  $\psi_{sx}$  is strictly greater than zero for any working condition. Thus, the condition  $\psi_{sx} > 0$  ensures that the mapping  $h_2^{-1}(x)h_1(x)$  is a diffeomorphism, i.e. it is an invertible function that maps one differentiable manifold to another, so that both the function and its inverse are smooth.

*Remark 2:* Note that the complication of considering the auxiliary input  $\nu_x$  in the definition of the state feedback to linearize the speed dynamics has never been considered and tested in past works. This problems comes from the fact

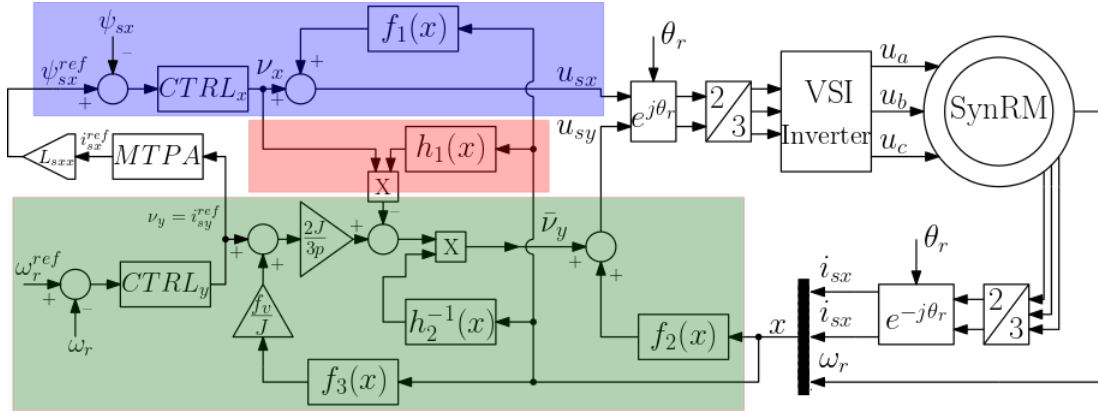


Figure 4. Block diagram of the proposed controller.

that self and cross-saturation effects in the model imply the dependency of the inductances on the stator current.

The block diagram of the suggested control scheme is shown in Fig. 4. Where they are highlighted with blue color the part related with direct axis flux control, with green color the part related with speed control, and with red color how the auxiliary input  $\nu_x$  enters for linearizing the speed dynamics.

#### A. Computation Requirement of the FL

As for the online computational effort, it is certainly higher with the proposed *FLC* than that required by the classic *FOC*. Both *FL* and *FOC* require the vector rotations from and to the synchronous reference frame. Both of them require a flux model (or observer) if closed-loop flux control is to be performed. The difference between the two lies primarily in the nonlinear transformations (14) and (18). As for the magnetic model that is embedded in the *FL* controller, all the analytical functions defining it, that are highly nonlinear and computationally demanding, once the model is identified offline, have been implemented online as linearly interpolated look-up tables, thus significantly reducing the overall computational effort. In particular the turnaround time has been evaluated in both cases, which is strictly related to the execution time of the code. It is  $8 \cdot 10^{-6}$  s for the *FOC* and  $10^{-5}$  s for the proposed *FL*, which means that the required execution time is only 20% higher. This percentage can probably further reduced optimizing the control code. It is noteworthy that the measurement of the execution time, or “turnaround time” as called in DS1103 interface, is an actual measurement, not an estimation: it is the actual time that the board uses to complete a computational cycle of the application loaded onto the board itself.

#### B. Controller design

In Fig. 4 the controller called  $CTRL_x$  is a PI-type controller designed to assign a suitable closed loop dynamics to the system (15), while the controller called  $CTRL_y$  is a PID-type controller designed to assign a suitable closed loop dynamics to the system (23). The two controllers are driven by the direct axis flux and rotor speed errors respectively. Note that the

two controllers can be designed independently of each other, so that the respectively error dynamics can be asymptotically stable.

In particular, for direct axis flux dynamics, a PI controller has been adopted, whose transfer function is given by:

$$G_{c,\psi} = k_{p,\psi} + \frac{k_{i,\psi}}{s}. \quad (25)$$

Although system (15) already contains a pole in  $s = 0$ , a PI controller (which introduces a further pole in  $s = 0$  and a zero in  $s = \frac{k_{i,\psi}}{k_{p,\psi}}$ ) is employed, because system (15) is obtained only for a perfect parameters knowledge. As a consequence, if the integral action is not included in the controller, non-zero steady-state errors can occur. In this way, the system is more robust against parameter uncertainties. This is an important theoretical issue has been further demonstrated in the tests shown in Subsection V.C. For speed dynamics, a PID controller has been adopted, whose transfer function is given by:

$$G_{c,\omega} = k_{p,\omega} + \frac{k_{i,\omega}}{s} + \frac{k_{d,\omega}s}{1 + \frac{k_{d,\omega}}{k_{p,\omega}N}s}, \quad (26)$$

with  $N > 10$ . In this case an integral action has been included for robustness reasons. However, since the speed dynamics is governed by a double integrator (see (23)), a derivative action is necessary to ensure stability of the closed loop system and give a positive contribution to the phase to assign a suitable phase margin.

To verify the improvements in the dynamic performance achievable with the adoption of the proposed control technique, it will be compared with the industrial standard in high performance control of *SynRM* drives: the Field Oriented Control (*FOC*). Among the different *FOC* algorithms, the *ROC* has been adopted here for comparison purposes. In details, to compare the feedback linearization control to the *ROC*, the controller parameters  $k_{p,\psi}$ ,  $k_{i,\psi}$ ,  $k_{p,\omega}$ ,  $k_{i,\omega}$  and  $k_{d,\omega}$ , and the parameters of the PI in the *ROC* should be chosen so that the two closed loop systems present the same dynamics. In this case, the same crossing pulsation  $\bar{\omega}_t$  and the same phase margin  $\bar{m}_\phi$  are imposed, by designing the controller so that:

$$|G_c(j\bar{\omega}_t)| |G_p(j\bar{\omega}_t)| = 1, \quad (27a)$$

$$\arg(G_c(j\bar{\omega}_t)) + \arg(G_p(j\bar{\omega}_t)) + \pi = \bar{m}_\phi, \quad (27b)$$

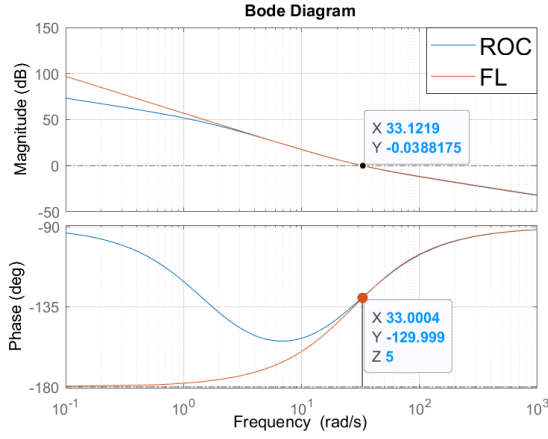


Figure 5. Bode Diagram: open-loop transfer function for direct axis flux dynamics.

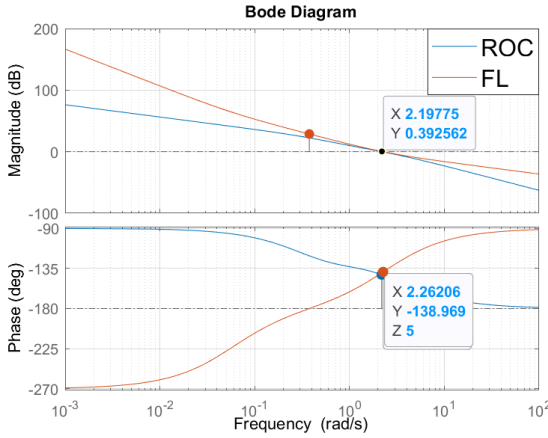


Figure 6. Bode Diagram: open-loop transfer function for speed dynamics.

where  $\bar{\omega}_t$  and  $\bar{m}_\phi$  are the design crossing pulsation and phase-margin, respectively,  $G_c(\cdot)$  is either (25) or (26), and  $G_p(\cdot)$  is either (15) or (23). It should be noted that, while in the proposed *FLC* the controlled variable is the direct axis flux, in *ROC* the controlled variable is the direct axis current. To make the design of the control systems of *FLC* and *ROC* with equal closed loop bandwidth, it has been assumed that the controlled variable of the rotor oriented control is the direct axis flux, computed on the basis of the direct axis self-inductance at the rated current. Afterwards, the direct current controller gains have been scaled according to the constant gain introduced by the direct axis self-inductance, so to guarantee that the closed loop bandwidth of the two controllers are equal.

Using the controllers tuned with the parameters given in Table II, for both *ROC* and *FL*, the Bode diagrams of the transfer functions of the open-loop systems, plotted in Figs. 5 and 6, are obtained. From these figures, it can be easily observed that the two systems, respectively *SynRM* controlled with *FL* and *SynRM* controlled with *ROC*, have the same crossing pulsation and the same phase margin, as shown in Table III. Moreover, Figs. 7 and 8 show the Bode diagrams of the closed-loop transfer functions. From these figures, it is possible to see that the same closed loop bandwidths are

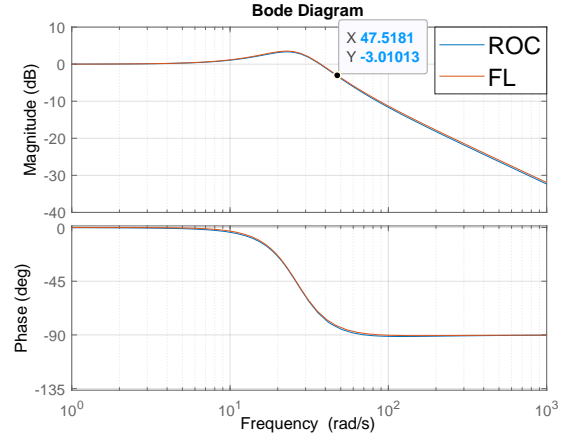


Figure 7. Bode Diagram: closed-loop transfer functions of the direct axis flux dynamics.

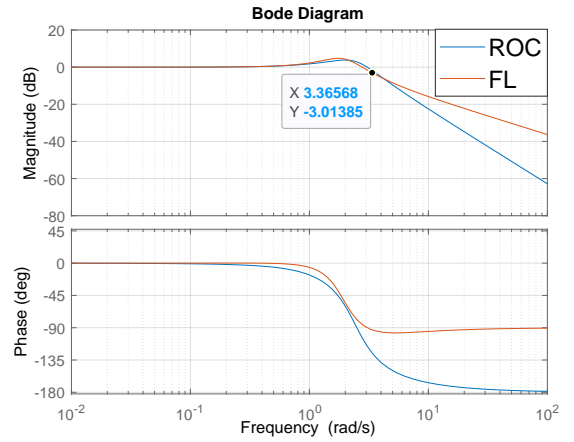


Figure 8. Bode Diagram: closed-loop transfer functions of the speed dynamics.

obtained, equal to about  $B_{-3\text{dB}} = 47.5$  rad/s for the direct axis flux loop and  $B_{-3\text{dB}} = 3.37$  rad/s for the speed loop. Figs. 5 and 6 clearly show that the controllers have been designed so to guarantee a phase margin of 45 degrees and a gain margin equal to infinity for both the controllers. It inherently implies the stability of the system. Moreover, the definition of the nonlinear transformation of the states and inputs in eq.s (14) and (18) guarantees that such stability margin is guaranteed in each operating condition, independently from the magnetic saturation.

However to obtain the transfer functions in the *ROC* case, the assumptions of constant parameters and constant direct axis flux amplitude should be made. In particular, for the transfer function of the flux, as well as for the transfer function of the speed, the parameters obtained at rated currents are considered. This represents a limitation for the *ROC* as compared with the *FL*: in the *FL* the specifics given in Table III are satisfied in all working conditions, while in the *ROC* these specifics could change if the flux level is different from the rated one (condition always happening under *MTPA*). They are therefore rigorously respected in one only working condition. This fact is evident, because if the motor is controlled by *FLC*



Table II  
PARAMETERS OF THE CONTROLLERS

ROC		FL	
Direct flux-loop	Speed-loop	Direct flux-loop	Speed-loop
$k_{p,\psi} = 24.2$	$k_{p,\omega} = 0.15$	$k_{p,\psi} = 25.3$	$k_{p,\omega} = 3.86$
$k_{i,\psi} = 723$	$k_{i,\omega} = 0.30$	$k_{i,\psi} = 700$	$k_{i,\omega} = 0.22$
			$k_{d,\omega} = 1.53$

Table III  
DESIGN SPECIFICS

	SPEED	DIRECT FLUX
Crossing pulsation	$\bar{\omega}_t = 2.2$ rad/s	$\bar{\omega}_t = 33$ rad/s
Phase margin	$m_\phi = 38^\circ$	$m_\phi = 50^\circ$

the closed loop transfer function can be deduced from (15) and (23) where no physic parameters appear, while if the motor is controlled by *ROC* the closed loop transfer function contains the machine parameters that are varying with currents, due to the saturation effects (e.g. the inductances in (4), (5) and (6)).

### C. Comparison between the proposed FL and ROC

The proposed *FL* overcomes *ROC* in terms of performance in both constant direct axis flux and variable direct axis flux working conditions. The reason why it overcomes *ROC* in variable direct axis flux conditions is that it can cover the non-linearity due to the torque expression. In fact, a coupling exists between the speed and the direct axis current (direct axis flux) loops, and a related non-linearity in the system, between the direct ( $x$ ) and quadrature ( $y$ ) axis in variable flux working condition due to fact that the electromagnetic torque is proportional to the product between the direct and quadrature current components. The capability of correctly decoupling the speed and the direct axis current (flux) loops in variable direct axis flux working conditions is a standard prerogative of *FL*, while it is not of *ROC* [10]. The reason why the proposed *FL* overcomes *ROC* even in constant direct axis flux conditions is that it can cover the non-linearity due to the magnetic saturation, that is a peculiar prerogative of this specific version of *FL*. Thanks to this feature, the controlled system presents always the same dynamics with a controller characterized by a fixed structure, independently from the operating point (independently from the flux and load values). This is not the case of the *ROC*, presenting a dynamics variable with the operating conditions, because of the variations of the inductances with the magnetic saturation.

Table IV  
PARAMETERS OF THE *SynRM* SATURATION MODEL

SYMBOL	VALUE	SYMBOL	VALUE
$\alpha_1$	1.2139	$\gamma$	0.156
$\beta_1$	0.4848	$\mu_1$	2.161
$\eta_1$	0.0111	$\sigma_1$	0.622
$\alpha_2$	0.3609	$\mu_2$	3.343
$\beta_2$	0.4033	$\sigma_2$	0.971
$\eta_2$	0.0042	$R_0$	8142

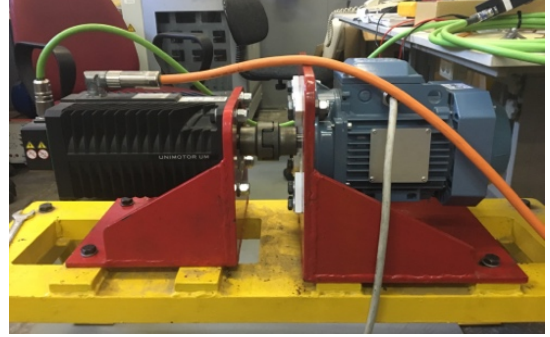


Figure 9. Photograph of the *SynRM* experimental set-up.

Table V  
RATED DATA OF THE *SYNRM*

SYMBOLS	VALUES
Rated power (kW)	2.2
Rated voltage (V)	380
Rated frequency (Hz)	50
Pole-pairs	2
Rated speed (rpm)	1500
Rated current (A)	5.5
Rated torque (Nm)	14

### IV. TEST SET-UP

The employed test set-up consists of a *SynRM* motor ABB 3GALO92543-BSB whose rated data are given in Table V. Table IV shows the parameters of the complete saturation model, identified with the technique proposed in [32]. The *SynRM* is supplied by a Voltage Source Inverter (*VSI*) with insulated gate bipolar transistor (*IGBT*) modules, model Semikron SMK 50 GB 123, driven by a Space-Vector Pulse Width Modulation (*SV-PWM*) technique with PWM frequency set to 5 kHz. The adopted control technique has been implemented on a dSPACE card (DS1103) with a PowerPC 604e at 400 MHz and a fixed-point DSP TMS320F240. The sampling time of controller has been set to 10 kHz. The *SynRM* motor is mechanically coupled to a torque controlled permanent magnet synchronous motor drive working as active load. Fig. 9 shows the photo of the *SynRM* drive test set-up.

### V. EXPERIMENTAL RESULTS

The proposed *FLC* technique, specifically developed for *SynRM* drives, has been experimentally compared with the *ROC*. The test set-up described in Section IV has been exploited for this purpose. As for the adopted version of the *ROC*, a rotor oriented control has been used [5]. Both the *FLC* and the *ROC* controllers have been tuned so to present the same dynamic performance, as fully explained in Section III.A. Moreover, some tests have been made in constant flux and other in variable flux working condition. As for the variable flux operation, the *SynRM* drive has been integrated the Maximum Torque Per Ampere (*MTPA*) technique proposed in [18]. This is a very challenging working condition, in which *FLC* is theoretically expected to overcome *ROC* in terms of dynamic performance. As for the field weakening (constant power) and *MPTV* (reduced power) working regions, [33] clearly highlights that field weakening and *MPTV* can be

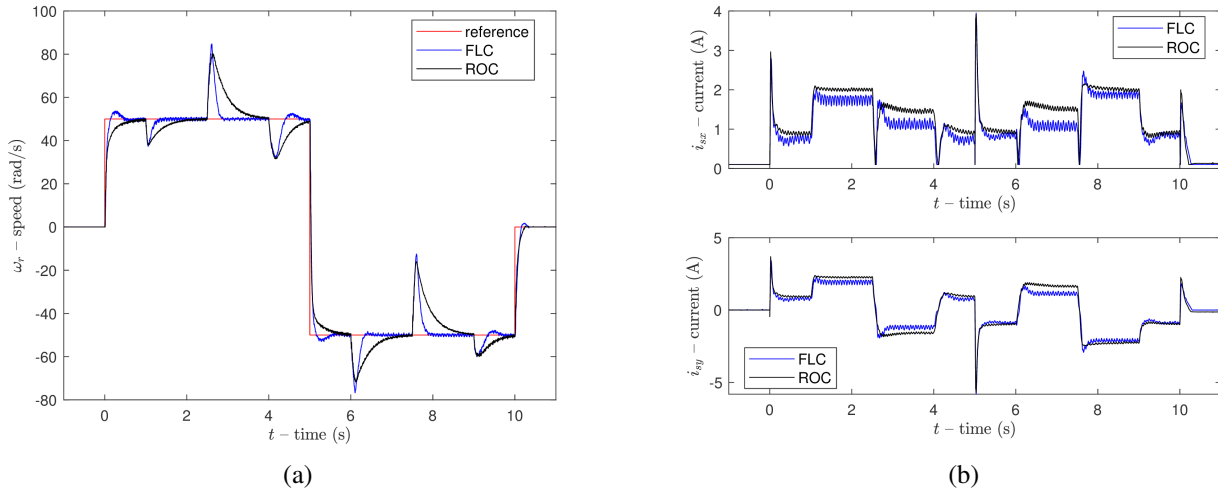


Figure 10. Reference and measured speed (a) and currents  $i_{sx}$  and  $i_{sy}$  (b), during a 4-quadrant test with contemporary variation of flux and load.

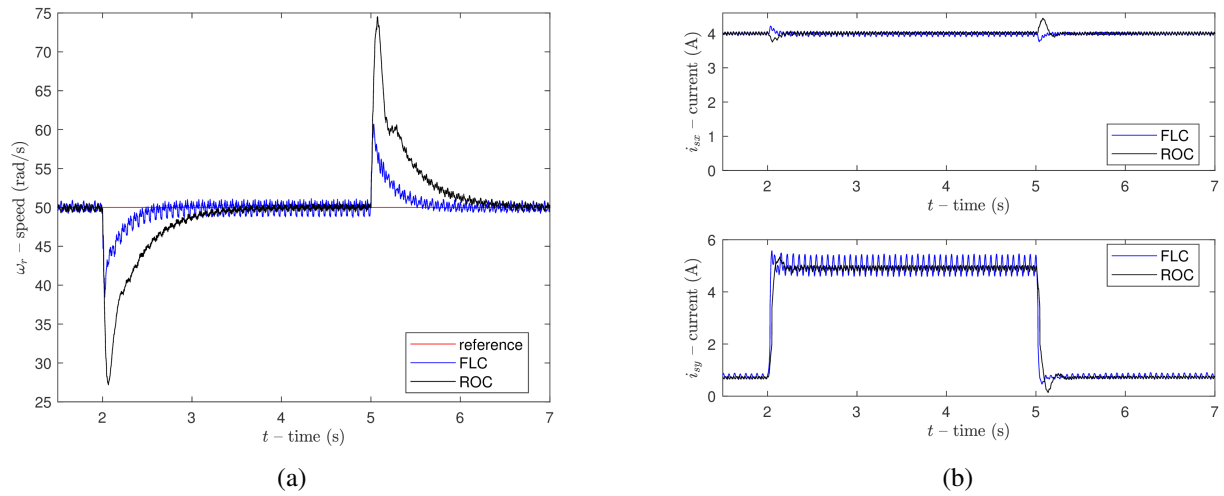


Figure 11. Reference and measured speed (a) and currents  $i_{sx}$  and  $i_{sy}$  (b), during a test with constant flux and speed, and load steps.

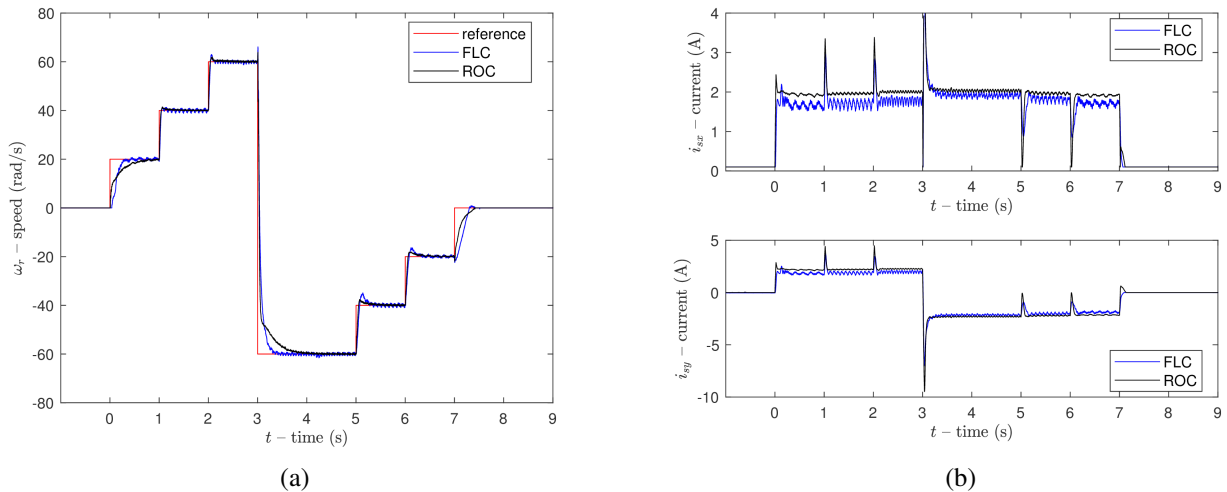


Figure 12. Reference and measured speed (a) and currents  $i_{sx}$  and  $i_{sy}$  (b), during a test with speed steps and MTPA conditions, at load.

performed regulating the direct component of the stator current (exactly with the same logic of *MTPA*). Such an approach could be thus easily integrated in the proposed *FLC* to cover the reduced power speed range. This is, however, out of the scope of this paper. Test 1 is a 4-quadrant test. Such a test has been performed in variable flux working conditions. The *SynRM* drive, starting from zero speed, has been firstly given a speed step reference of 50 rad/s at no-load. Once the drive has properly tracked the reference speed a load step torque of 2.5 Nm is applied (corresponding to 25% of the rated load), exploiting the *PMSM* drive as active load. Once the speed controller has governed the drive speed back to its reference, the load torque is modified with a step from 2.5 Nm to -2.5 Nm (making the drive work in regenerative mode). Afterwards, the load is released and a speed reversal from 50 rad/s to -50 rad/s commanded at no load. Once the drive has tracked the reference speed of -50 rad/s a step load torque of 2.5 Nm is firstly applied (making the drive work in regenerative mode) after which a load step of -2.5 Nm is applied. Fig. 10(a) shows the reference and measured speeds, obtained respectively with the proposed *FLC* and with the *ROC*. Fig. 10(b) shows the corresponding waveforms of the  $i_{sx}$ ,  $i_{sy}$  stator current components. The speed waveform show clearly that both the proposed *FLC* and the *ROC* guarantee very a fast dynamic response as well as a null steady-state tracking error. The dynamic performance achieved with the proposed *FLC* is, however, better than that obtained with *ROC*. The rise time obtained with the *FLC* is clearly lower, even if theoretically both *FLC* and *ROC* present the same closed loop bandwidth. Fig. 13 shows the *IAE* (Integral Absolute Error), as well as the overshoots and rise-times/settling times computed on the speed loop. It confirms that the *IAE* presented by the *FLC* is always much lower than that presented by *ROC*, almost one order smaller in all cases. They clearly highlight that *FLC* significantly overcomes *ROC* in terms of dynamic performance in both transient response and load rejection capability. As for the stator current waveforms,  $i_{sy}$  presents a step-wise waveform with positive (negative) peaks at either each positive (negative) variation of the reference speed or positive (negative) step of load torque. Correspondingly, even  $i_{sx}$  present the same shape, with an increase of  $i_{sx}$  at each speed step, because of the *MTPA*. It can be observed a slightly different value of  $i_{sx}$  with the *FLC* and *ROC*, that is due to the set of nonlinear transformation present in the *FLC*, not present in *ROC* where a cascaded loops control is operated. Test 2 is a load rejection test. Such a test has been performed in constant flux working conditions. The *SynRM* drive is operated at the constant speed of 50 rad/s. A step load torque of 10 Nm has been firstly applied and then released to the *SynRM* drive. The test has been performed with the machine magnetized at constant level ( $i_{sx} = 4.5$  A). Fig. 11(a) shows the reference and measured speeds, obtained respectively with the proposed *FLC* and with the *ROC*. Fig. 11(b) shows the corresponding waveforms of the  $i_{sx}$ ,  $i_{sy}$  stator current components. It can be clearly observed that, even in constant flux operation, *FLC* presents a far better load rejection than that presented by *ROC*: after the application or release of the load torque, the measured speed approaches its reference much faster in the *FLC* case

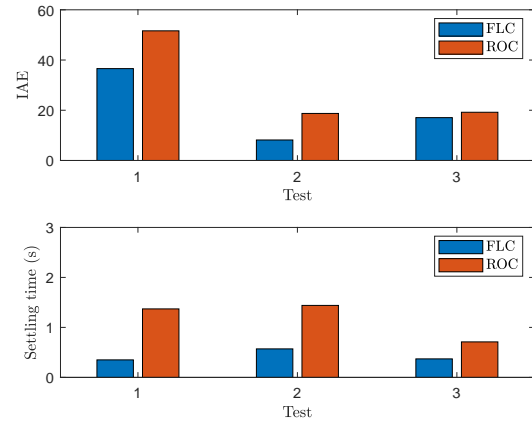


Figure 13. Performances indexes.

than in the *ROC* one. These results are consistent with what expected theoretically, confirmed by the *IAE* indexes and settling times shown in Fig. 13. Test 3 is a fast speed-transient test at light load. Such a test has been performed in variable flux working conditions. A set of speed step references including a speed reversal, of the type  $0 \rightarrow 20 \rightarrow 40 \rightarrow 60 \rightarrow -60 \rightarrow -40 \rightarrow -20 \rightarrow 0$  rad/s has been given the drive, while it is subjected to a constant load equal to 2.5 Nm, corresponding to 25% of the rated load. Fig. 12(a) shows the reference and measured speeds, obtained respectively with the proposed *FLC* and with the *ROC*. Fig. 12(b) shows the corresponding waveforms of the  $i_{sx}$ ,  $i_{sy}$  stator current components. It can be observed that both *FLC* and *ROC* present good dynamic performance in speed control. The measured speed correctly tracks its reference with a low rise time and null tracking error. Since the drive is constantly loaded with 25% of the rated torque, it can accelerate/decelerate exploiting just the difference between the maximum torque and the load one. This is the reason why *FLC* outperforms *ROC* less in this test than in the former ones, as clearly emphasized by the *IAE* index in Fig. 13.

Finally, the last test is related to rated load - rated speed operation under *MTPA*. The *SynRM* drive has been given a reference speed equal to the rated speed of 150 rad/s at no load. Afterwards, at  $t = 2$  s a step torque equal to the rated load of 14 Nm has been applied, exploiting the *PMSM* drive as active load. Fig. 14a shows the reference and measured speed during this test, while Fig. 14b shows the corresponding  $i_{sx}$ ,  $i_{sy}$  current components. The speed curve shows that the measured speed correctly tracks its reference at no load. As soon as the rated step torque is applied to the drive, the measured speed reduces but the control system suddenly reacts increasing the electromagnetic torque so that in less than 1 s the measured speed gets its reference. The dual situation happens as soon as the load rated torque is released. The current waveforms are coherent with the speed one. While the drive is running at no load,  $i_{sy}$  is controlled at a minimum value permitting to cope the mechanical friction losses. When the rated load is applied,  $i_{sy}$  increases suddenly in order to compensate the load. According to the *MTPA* logic,  $i_{sx}$  presents almost the same shape of  $i_{sy}$ . All these figures witness the correct load rejection capability of the drive at rated values.

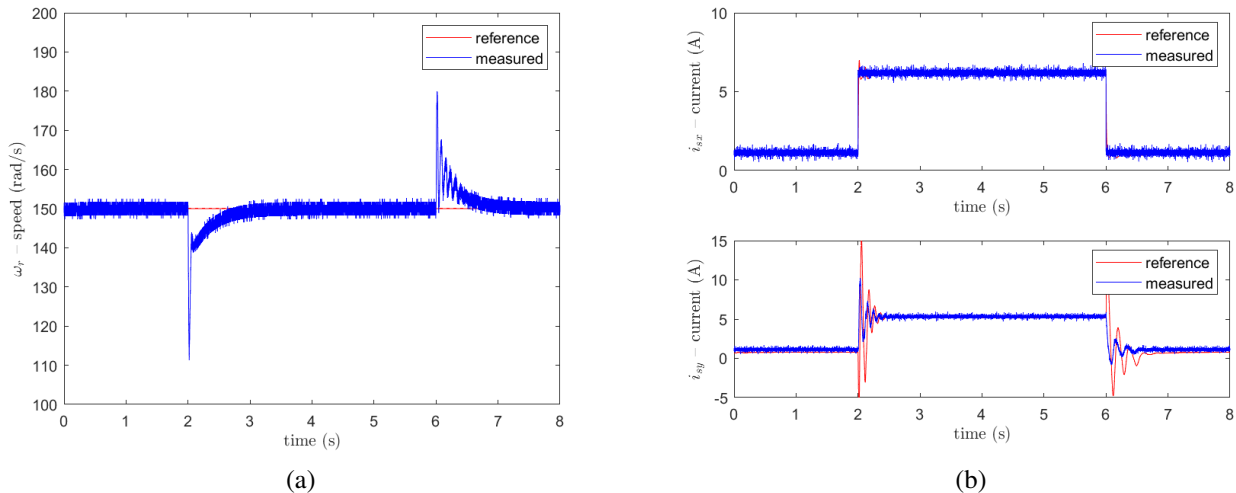


Figure 14. Reference and measured speed (a) and currents  $i_{sx}$  and  $i_{sy}$  (b) during rated load - rated speed operation.

#### A. FLC behavior under detuned working conditions

Input-output feedback linearization is a very powerful non-linear control technique, theoretically guaranteeing better dynamic performance than *ROC* (or *FOC*). *FLC*, however, strongly relies on two aspects:

- the accuracy of the model underlying the *FLC*; for this reason, a dynamic model accounting for the magnetic saturation including cross-saturation has been suitably defined and exploited.
- the correctness of the model's parameters; with this regard a specific parameter estimation technique has been developed permitting all the model parameters to be properly identified [32].

In general, the imperfect knowledge of the model's parameters causes the presence of a non-null tracking error and a modification of the dynamic performance of the *FLC* controller. Such effects are quite hardly predictable in advance. In order to verify the sensitivity of the proposed *FLC* versus the variation of the main parameters of the *SynRM* model, some tests have been performed under strongly detuned working conditions. The sensitivity of the proposed *FLC* versus the variation of  $R_s$ ,  $L_{sxx}$ ,  $L_{syy}$  has been analyzed. In particular  $R_s$  has been varied of 100%, while  $L_{sxx}$  and  $L_{syy}$  have been varied of  $\pm 50\%$ . Three operating speeds have been chosen: 10 rad/s (low speed), 100 rad/s (below rated speed), 200 rad/s (field weakening).

Fig. 15 shows the reference and measured speed as well as the direct axis current with the *FLC*. With the controller properly tuned, the *FLC* exhibits the expected dynamic behavior, in accordance with the controller design described in section III.A. Moreover, the steady-state tracking errors of both the speed and direct axis loops are null, because of the chosen linear controller has a pole in the origin of the complex plane.

Fig. 16 shows the case of  $\pm 50\%$  of variation of  $L_{sxx}$ . The same test has been made at 10 rad/s (low speed), 100 rad/s (below rated speed) and 200 rad/s (field weakening). Figs 17 and 18 shows the same kinds of waveform related to the variations of  $L_{syy}$  and  $R_s$ . These figures clearly show that

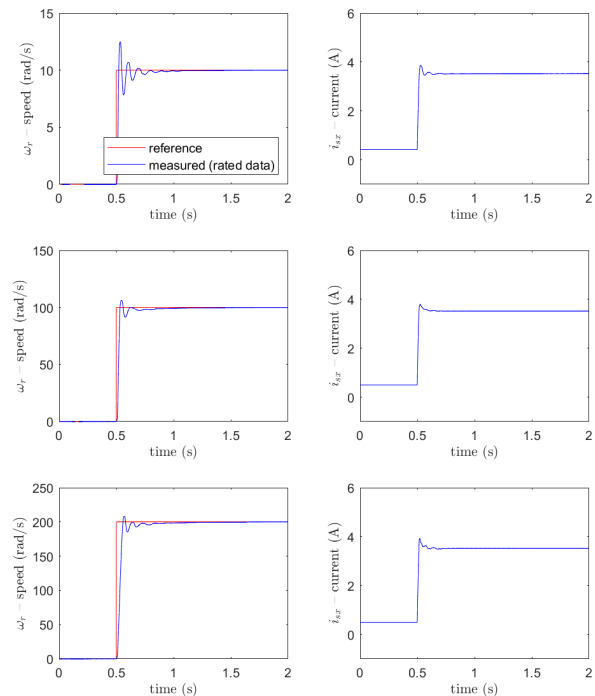


Figure 15. Reference and measured speed, direct axis current with the *FLC* properly tuned.

the effects of the detuning of  $L_{sxx}$  is almost negligible at low speed, while it is visible at medium speed and becomes critical at high speed, in particular in field weakening, as expected. The effect is more visible on the current than on the speed. As for  $L_{syy}$ , the effect of the detuning is perfectly observable even at low speed becoming significant at increasing speeds, with critical oscillations of both the speed and current. The detuning of the stator resistance presents a dual behaviour. It is almost negligible at high speed, while it becomes significant

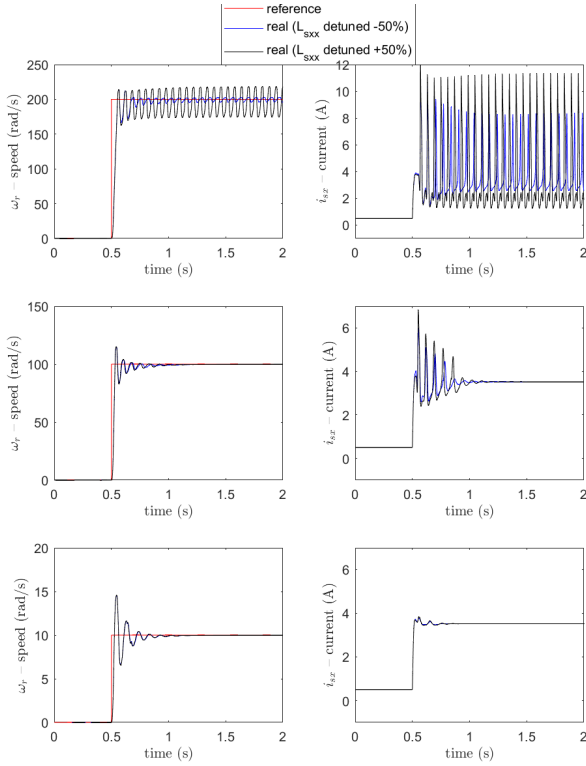


Figure 16. Reference and measured speed, direct axis current with the *FLC* with the  $L_{sxx}$  and  $L'_{sxx}$  detuned of  $\pm 50\%$ .

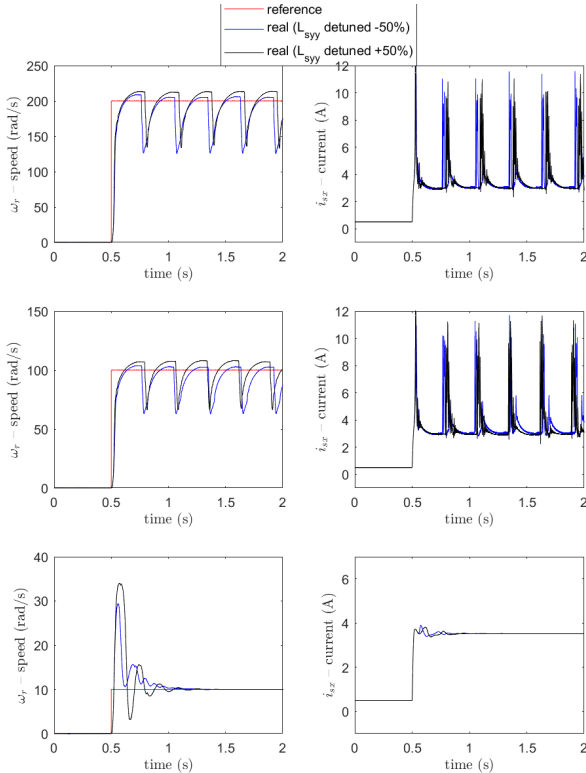


Figure 17. Reference and measured speed, direct axis current with the *FLC* with the  $L_{syy}$  and  $L'_{syy}$  detuned of  $\pm 50\%$ .

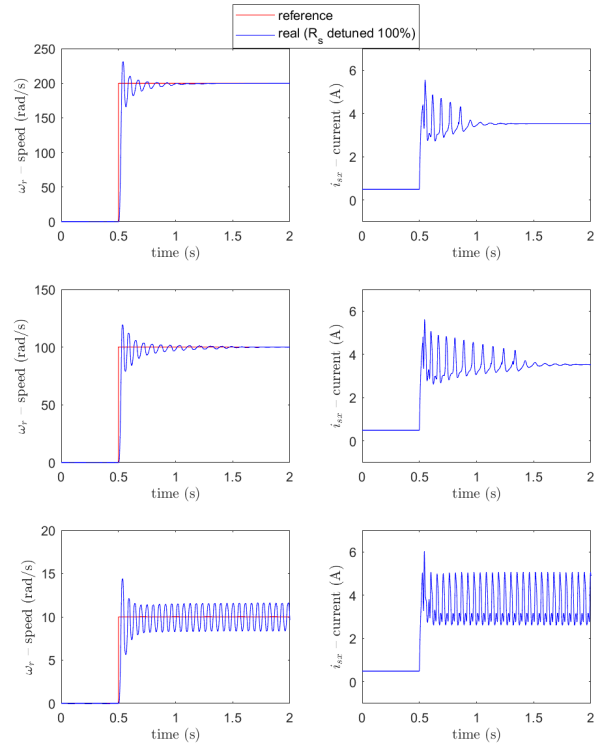


Figure 18. Reference and measured speed, direct axis current with the *FLC* with the  $R_s$  detuned of 100%.

at low speed. The above figures clearly show that the imperfect knowledge of the inductances can be very critical for the control performance and thus fully justify the integration of a suitably developed magnetic model in the proposed *FLC*.

It should be finally noted that the steady state error is null, even in presence of a strong detuning of the parameters. This is due to the chosen structure of the controller.

## VI. CONCLUSION

This paper proposes a nonlinear controller based on input-output feedback linearization for *SynRMs* motor drives that takes into consideration the magnetic saturation. The proposed nonlinear *FL* based control technique has been developed starting from the theoretical definition of an original dynamic model of the *SynRM* taking into consideration both the self and the cross-saturation effects. Such control technique permits the dynamics of both the speed and flux loops to be maintained constant independently of the load and the saturation of the iron core in both constant flux and variable flux operating conditions. The proposed technique has been tested experimentally on a suitably developed test set-up. It has been further experimentally compared with *FOC* in both constant and variable flux operation, exhibiting better dynamic performance in both working conditions. Finally, the limited degradation of the performance of the proposed *FLC* versus the variation of the main motor parameters has been further verified.

## ACKNOWLEDGEMENT

This work was partially supported by the USP-SRT Research Project: Advanced Control of Synchronous Reluctance Motors for Electrical Vehicles (ACOSREV).

## APPENDIX

$$l_{xx} = \frac{\gamma}{\sigma_1} \frac{\operatorname{sgn}(i_{sx})}{\left( e^{\frac{(i_{sx} - \mu_1 \operatorname{sgn}(i_{sx})) \operatorname{sgn}(i_{sx})}{2\sigma_1}} + e^{-\frac{(i_{sx} - \mu_1 \operatorname{sgn}(i_{sx})) \operatorname{sgn}(i_{sx})}{2\sigma_1}} \right)^2},$$

$$l_{xy} = \frac{1}{1 + e^{-\frac{(i_{sy} - \mu_2 \operatorname{sgn}(i_{sy})) \operatorname{sgn}(i_{sy})}{\sigma_2}}},$$

$$l_{yy} = \frac{\gamma}{\sigma_2} \frac{\operatorname{sgn}(i_{sy})}{\left( e^{\frac{(i_{sy} - \mu_2 \operatorname{sgn}(i_{sy})) \operatorname{sgn}(i_{sy})}{2\sigma_2}} + e^{-\frac{(i_{sy} - \mu_2 \operatorname{sgn}(i_{sy})) \operatorname{sgn}(i_{sy})}{2\sigma_2}} \right)^2},$$

$$l_{yx} = \frac{1}{1 + e^{-\frac{(i_{sx} - \mu_1 \operatorname{sgn}(i_{sx})) \operatorname{sgn}(i_{sx})}{\sigma_1}}},$$

$$l'_x = \frac{e^{\frac{(i_{sx} - \mu_1 \operatorname{sgn}(i_{sx})) \operatorname{sgn}(i_{sx})}{2\sigma_1}} - e^{-\frac{(i_{sx} - \mu_1 \operatorname{sgn}(i_{sx})) \operatorname{sgn}(i_{sx})}{2\sigma_1}}}{e^{\frac{(i_{sx} - \mu_1 \operatorname{sgn}(i_{sx})) \operatorname{sgn}(i_{sx})}{2\sigma_1}} + e^{-\frac{(i_{sx} - \mu_1 \operatorname{sgn}(i_{sx})) \operatorname{sgn}(i_{sx})}{2\sigma_1}}},$$

$$l'_y = \frac{e^{\frac{(i_{sy} - \mu_2 \operatorname{sgn}(i_{sy})) \operatorname{sgn}(i_{sy})}{2\sigma_2}} - e^{-\frac{(i_{sy} - \mu_2 \operatorname{sgn}(i_{sy})) \operatorname{sgn}(i_{sy})}{2\sigma_2}}}{e^{\frac{(i_{sy} - \mu_2 \operatorname{sgn}(i_{sy})) \operatorname{sgn}(i_{sy})}{2\sigma_2}} + e^{-\frac{(i_{sy} - \mu_2 \operatorname{sgn}(i_{sy})) \operatorname{sgn}(i_{sy})}{2\sigma_2}}}.$$

## REFERENCES

- [1] A. Accetta, M. Cirrincione, M. Pucci, and A. Sferlazza, "A nonlinear control of synchronous reluctance motors (SynRM) based on feedback linearization considering the self and cross-saturation effects," in *Energy Conversion Congress and Exposition*, pp. 1804–1809, IEEE, 2019.
- [2] P. Vas, *Sensorless vector and direct torque control*. Oxford university press Oxford, UK, 1998.
- [3] L. Xu, X. Xu, T. A. Lipo, and D. W. Novotny, "Vector control of a synchronous reluctance motor including saturation and iron loss," *IEEE Transactions on Industry Applications*, vol. 27, no. 5, pp. 977–985, 1991.
- [4] R. E. Betz, R. Lagerquist, M. Jovanovic, T. J. Miller, and R. H. Middleton, "Control of synchronous reluctance machines," *IEEE Transactions on Industry Applications*, vol. 29, no. 6, pp. 1110–1122, 1993.
- [5] A. Vagati, M. Pastorelli, and G. Franceschini, "High-performance control of synchronous reluctance motors," *IEEE Transactions on Industry Applications*, vol. 33, no. 4, pp. 983–991, 1997.
- [6] K. Uezato, T. Senjyu, and Y. Tomori, "Modeling and vector control of synchronous reluctance motors including stator iron loss," *IEEE Transactions on Industry Applications*, vol. 30, no. 4, pp. 971–976, 1994.
- [7] G. Pellegrino, R. I. Bojoi, and P. Guglielmi, "Unified direct-flux vector control for AC motor drives," *IEEE Transactions on Industry Applications*, vol. 47, no. 5, pp. 2093–2102, 2011.
- [8] H. K. Khalil, *Nonlinear systems*, vol. 3. Prentice Hall, 2002.
- [9] A. Isidori, *Nonlinear control systems, (third edition)*. Springer, 1995.
- [10] R. Marino, P. Tomei, and C. M. Verrelli, *Induction motor control design*. Springer Science & Business Media, 2010.
- [11] R. Marino, S. Peresada, and P. Valigi, "Adaptive input-output linearizing control of induction motors," *IEEE Transactions on Automatic control*, vol. 38, no. 2, pp. 208–221, 1993.
- [12] C. Lascu, S. Jafarzadeh, M. S. Fadali, and F. Blaabjerg, "Direct torque control with feedback linearization for induction motor drives," *IEEE Transactions on Power Electronics*, vol. 32, no. 3, pp. 2072–2080, 2016.
- [13] H. A. Zarchi, J. Soltani, A. Maleknia, and G. R. A. Markadeh, "A Lyapunov based nonlinear speed tracking controller for synchronous reluctance motor using adaptive input-output feedback linearization technique," in *International Conference on Industrial Technology*, pp. 1–5, IEEE, 2008.
- [14] H. A. Zarchi, J. Soltani, and G. A. Markadeh, "Adaptive input-output feedback-linearization-based torque control of synchronous reluctance motor without mechanical sensor," *IEEE Transactions on Industrial Electronics*, vol. 57, no. 1, pp. 375–384, 2010.
- [15] H.-D. Lee, S.-J. Kang, and S.-K. Sul, "Efficiency-optimized direct torque control of synchronous reluctance motor using feedback linearization," *IEEE Transactions on Industrial Electronics*, vol. 46, no. 1, pp. 192–198, 1999.
- [16] M. Nabipour, H. A. Zarchi, and S. Madani, "Robust position control of synchronous reluctance motor drives using linear variable structure and adaptive input-output feedback linearization approaches," in *Iranian Conference on Electrical Engineering*, pp. 1–5, IEEE, 2011.
- [17] H. A. A. Awan, M. Hinkkanen, R. Bojoi, and G. Pellegrino, "Stator-flux-oriented control of synchronous motors: A systematic design procedure," *IEEE Transactions on Industry Applications*, vol. 55, no. 5, pp. 4811–4820, 2019.
- [18] A. Accetta, M. Cirrincione, M. C. Di Piazza, G. La Tona, M. Luna, and M. Pucci, "Analytical formulation of a maximum torque per ampere (MTPA) technique for SynRMs considering the magnetic saturation," *IEEE Transactions on Industry Applications*, vol. 56, no. 4, pp. 3846–3854, 2020.
- [19] A. Accetta, M. Cirrincione, M. Pucci, and A. Sferlazza, "A space-vector state dynamic model of the synchronous reluctance motor including self and cross-saturation effects and its parameters estimation," in *Energy Conversion Congress and Exposition*, pp. 4466–4472, IEEE, 2018.
- [20] A. Accetta, M. Cirrincione, M. Pucci, and A. Sferlazza, "A saturation model of the synchronous reluctance motor and its identification by genetic algorithms," in *Energy Conversion Congress and Exposition*, pp. 4460–4465, IEEE, 2018.
- [21] Z. Qu, T. Tuovinen, and M. Hinkkanen, "Inclusion of magnetic saturation in dynamic models of synchronous reluctance motors," in *International Conference on Electrical Machines*, pp. 994–1000, IEEE, 2012.
- [22] H. De Jong, "Saturation in electrical machines," in *International Conference on Electrical Machines*, vol. 80, pp. 1545–1552, 1980.
- [23] K. Corzine, B. T. Kuhn, S. Sudhoff, and H. Hegner, "An improved method for incorporating magnetic saturation in the qd synchronous machine model," *IEEE Transactions on Energy Conversion*, vol. 13, no. 3, pp. 270–275, 1998.
- [24] C. Mademlis, "Compensation of magnetic saturation in maximum torque to current vector controlled synchronous reluctance motor drives," *IEEE Transactions on Energy Conversion*, vol. 18, no. 3, pp. 379–385, 2003.
- [25] T. Tuovinen, M. Hinkkanen, and J. Luomi, "Analysis and design of a position observer with resistance adaptation for synchronous reluctance motor drives," *IEEE Transactions on Industry Applications*, vol. 49, no. 1, pp. 66–73, 2012.
- [26] A. Kithau and J. Pacas, "Appropriate models for the control of the synchronous reluctance machine," in *Conference Record of the 2002 IEEE Industry Applications Conference*, vol. 4, pp. 2289–2295, IEEE, 2002.
- [27] S. Yamamoto, K. Tomishige, and T. Ara, "A method to calculate transient characteristics of synchronous reluctance motors considering iron loss and cross-magnetic saturation," in *Conference Record of the 2005 IEEE Industry Applications Conference*, vol. 3, pp. 1754–1761, IEEE, 2005.
- [28] E. Armando, P. Guglielmi, G. Pellegrino, M. Pastorelli, and A. Vagati, "Accurate modeling and performance analysis of IPM-PMASR motors," *IEEE Transactions on Industry Applications*, vol. 45, no. 1, pp. 123–130, 2009.
- [29] A. Vagati, M. Pastorelli, F. Scapino, and G. Franceschini, "Impact of cross saturation in synchronous reluctance motors of the transverse-laminated type," *IEEE Transactions on Industry Applications*, vol. 36, no. 4, pp. 1039–1046, 2000.
- [30] N. Bedetti, S. Calligaro, and R. Petrella, "Stand-still self-identification of flux characteristics for synchronous reluctance machines using novel saturation approximating function and multiple linear regression," *IEEE Transactions on Industry Applications*, vol. 52, no. 4, pp. 3083–3092, 2016.
- [31] H. Mahmoud, G. Bacco, M. Degano, N. Bianchi, and C. Gerada, "Synchronous reluctance motor iron losses: Considering machine nonlinearity at MTPA, FW, and MTPV operating conditions," *IEEE Transactions on Energy Conversion*, vol. 33, no. 3, pp. 1402–1410, 2018.
- [32] A. Accetta, M. Cirrincione, M. Pucci, and A. Sferlazza, "Space-vector state dynamic model of SynRM considering self-and cross-saturation and related parameter identification," *IET Electric Power Applications*, vol. 14, no. 14, pp. 2798–2808, 2021.
- [33] L. Sepulchre, M. Fadel, M. Pietrzak-David, and G. Porte, "MTPV flux-weakening strategy for PMSM high speed drive," *IEEE Transactions on Industry Applications*, vol. 54, no. 6, pp. 6081–6089, 2018.



**Angelo Accetta** (M'08) received his master's degree in Electrical Engineering in 2008, at the University of Palermo, where, in 2011, he obtained the Ph.D. in Electrical Engineering, in collaboration with the Institute for Studies on Intelligent Systems for Automation (ISSIA) - National Research Council (CNR). From 2013 to 2018 he was a Junior Researcher at the Section of Palermo of ISSIA-CNR, Palermo, Italy, working to new energy management strategies for distributed generation systems and to the implementation of new sensorless control strategies

for permanent magnets synchronous electric motors (PMSM) and for induction motors both rotating (RIM) and linear (LIM). He is currently Junior Researcher at the INstitute of Marine engineering (INM)-CNR. His research interest are sensorless control systems for electric drives with induction, rotating and linear, motors, with particular attention to their applications for electric generation systems and electric propulsion.

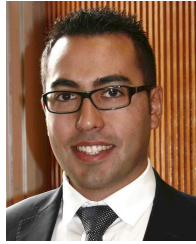


**Marcello Pucci** (M'03–SM'11) received the Laurea and Ph.D. degrees in electrical engineering from the University of Palermo, Italy, in 1997 and 2002, respectively. In 2000, he was a Host Student with the Institute of Automatic Control, Technical University of Braunschweig, Braunschweig, Germany, working in the field of control of ac machines, with a grant from the German Academic Exchange Service. From 2001 to 2018, he has been with the Institute of Intelligent Systems for Automation, Section of Palermo, National Research Council of Italy. Currently he is

a Senior Researcher at the INstitute of Marine engineering (INM)-CNR. His current research interests include electrical machines; control, diagnosis, and identification techniques of electrical drives; and intelligent control and power converters. Dr. Pucci serves as an Associate Editor for the IEEE transactions on industrial electronics and IEEE transactions on industry applications. He is a member of the Editorial Board of the Journal of Electrical Systems.



**Maurizio Cirrincione** (M'03–SM'10) received the Laurea degree in electrical engineering from the Polytechnic University of Turin, Turin, Italy, in 1991 and the Ph.D. degree in electrical engineering from the University of Palermo, Italy, in 1996. From 1996 to 2005, he was a Researcher with the ISSIA-CNR Section of Palermo (Institute on Intelligent Systems for Automation), Palermo, Italy. In September 2005, as a full Professor he join the University of Technology of Belfort-Montbéliard, Belfort, France. He is currently the Head of the "School of Engineering and Physics" of the University of the South Pacific in Suva, Fiji. His current research interests are neural networks for modeling and control, system identification, intelligent control, power electronics, renewable energy systems, and electrical machines and drives. Dr. Cirrincione was awarded the 1997 "E.R.Caianello" prize for the best Italian Ph.D. thesis on neural networks.



**Antonino Sferlazza** (S'12–M'15) was born in Palermo, Italy, in 1987. He received the Master degree in automation engineering and the Ph.D. degree in mathematics and automation from the University of Palermo, Italy, in 2011 and 2015 respectively. In 2013 he was visiting PhD student at University of California at Santa Barbara, CA, USA, in the field of modeling and analysis of stochastic hybrid systems. From 2016 to 2017 he join the University of Palermo as junior researcher. From 2017 to 2018 he was researcher are LAAS CNRS of Toulouse,

France, working in the field of control of power converter. He is currently a researcher in systems and control engineering at the University of Palermo. His research interests include the development of feedback control algorithms for nonlinear dynamical systems, optimization techniques, estimation of stochastic dynamical systems, and applications of control of electrical drives, power converters, and mechanical systems.